J Solid State Electrochem (2001) 5: 466–472
DOI 10.1007/s100080100197

ORIGINAL PAPER

Su-Il Pyun · Jeong-Nam Han

A contribution to the kinetics of hydrogen transport through Pd foil electrode during hydrogen extraction under self-discharge and potentiostatic conditions

Received: 3 September 2000 / Accepted: 18 January 2001 / Published online: 8 August 2001
© Springer-Verlag 2001

Abstract This paper contributes to the kinetics of hydrogen transport through the Pd foil electrode in 0.1 mol l^{-1} NaOH solution during the hydrogen extraction from the foil electrode under the self-discharge and potentiostatic conditions by the analysis of open-circuit potential and anodic current transients, respectively. The hydrogen oxidation rate calculated based upon the mixed potential theory just equals the rate of hydrogen self-discharge from the electrode during the OCP transient. When the electrode surface is subjected even to a constant discharging potential, the hydrogen concentration gradient at the surface is given by the Butler-Volmer equation combined with the decay in actual potential jump with time below the transition discharging potential; however, the constant hydrogen concentration condition is satisfied at the surface above this potential. By taking the hydrogen oxidation rate during the OCP transient and the two constraints during the anodic current transient as the boundary condition at the surface, the hydrogen concentration profile transients have been derived during the hydrogen extraction under the self-discharge and potentiostatic conditions, respectively.

Keywords Pd foil electrode · Open-circuit potential transient · Current transient · Hydrogen concentration profile transient · Boundary condition

Introduction

The hydrogen injection into and extraction from hydride-forming electrodes such as Pd [1], $LaNi_5$ [2], and Zr-based alloy [3] have been extensively studied because of the interest in their application to anode material for high energy density storage batteries. For a better understanding of the kinetics of hydrogen injection and extraction, it is necessary to establish the initial and boundary conditions for the hydrogen transport during the hydrogen injection and extraction.

However, in particular, the boundary condition for the hydrogen transport is not yet well established during the self-discharge process since the rate of hydrogen self-discharge resulting by the action of local cells during the open-circuit potential (OCP) transient is not accessible to measurement when the hydrogen pre-charged electrode comprises a lot of hydrogen containing local cells. Moreover, it is known [4, 5] that the hydrogen transport follows the Cottrell equation under potentiostatic condition during the hydrogen injection and extraction. However, non-Cottrell behavior has been often reported under even potentiostatic conditions [6, 7, 8].

Therefore the present work considers the kinetics of hydrogen transport through the Pd foil electrode precharged with hydrogen at –0.02 V(RHE) during hydrogen extraction from the electrode under self-discharge and potentiostatic conditions. For this purpose, OCP transient and anodic current transient were measured on Pd foil electrode in 0.1 mol l^{-1} NaOH solution and analyzed to obtain the appropriate boundary condition for hydrogen extraction under self-discharge and potentiostatic conditions, respectively. Based upon the appropriate boundary condition proposed, the hydrogen concentration profile transients have been calculated during hydrogen extraction under self-discharge and potentiostatic conditions.

Presented at the international conference "Solid State Chemistry 2000", 3–8 September 2000, Prague, Czech Republik

S.-I. Pyun (✉) · J.-N. Han
Department of Materials Science and Engineering,
Korea Advanced Institute of Science and Technology,
373-1 Kusong-Dong, Yusong-Gu, Taejon 305-701, Korea
E-mail: sipyun@mail.kaist.ac.kr

Experimental

The specimen was cut from 75 μm thick Pd sheet (Leech Co.) into foil with dimensions of 3 mm×90 mm. In order to remove residual stresses, the Pd foil specimen was annealed under a vacuum of 10^{-2} Pa at 650 °C for 2 h, followed by furnace cooling. It was then mechanically ground with #2000 SiC emery paper to eliminate

surface oxide films, followed by chemical etching in concentrated nitric acid for 30 s. In order to make one side an impermeable boundary, a 0.3 μm thick Au layer was sputtered onto one side of the electrode specimen since hydrogen solubility in Au is extremely low [9]. The other face of the foil electrode specimen was exposed 3 mm in width, 50 mm in length, and 150 mm^2 in area to the electrolyte.

A platinum wire and a saturated calomel electrode (SCE) were used as a counter electrode and a reference electrode, respectively. An aqueous 0.1 mol l^{-1} NaOH solution used as an electrolyte in this work was deaerated for 24 h by bubbling with purified argon gas before all electrochemical experiments. All potentials quoted in this work are referred to the value of the potential of reversible hydrogen electrode (RHE), which was measured to be about –0.90 V(SCE) in 0.1 mol l^{-1} NaOH solution [1].

In order to obtain reproducible data, a successive cyclic voltammetry was carried out in the potential range of –0.1 to 0.9 V(RHE) at a scan rate of 1 mV s^{-1} before the OCP and anodic current transients. After that, two kinds of Pd foil electrode specimen were first polarized at –0.02 V(RHE) for 2×10^3 s in 0.1 mol l^{-1} NaOH solution alike. The hydrogen pre-charging potential was then suddenly interrupted on one specimen and was then jumped to various discharging potentials ranging from 0.20 to 0.90 V(RHE) on another specimen. From this moment on, the resulting OCP and anodic current were recorded with time.

Results and discussion

Figure 1a shows the anodic current transient on a logarithmic scale, obtained by jumping from various hydrogen pre-charging potentials –0.15 to 0.15 V(RHE) to the hydrogen discharging potential 0.90 V(RHE). The value of hydrogen content δ in Pd foil electrode was calculated by integrating the measured anodic current transient with respect to discharging time t. Keeping in mind that the electrode specimen was subjected to –0.15 to 0.15 V(RHE) for 2×10^3 s, each pre-charging potential is regarded as the electrode potential E. The value of E is plotted in Fig. 1b against the value of δ. As hydrogen is extracted from the electrode, i.e., the value of δ, 6.8×10^{-3}, falls to zero, the value of E, –0.15 V(RHE), increases more rapidly to 0.15 V(RHE). It should be noted that above 0.15 V(RHE) the value of δ becomes to zero.

In this pre-charging potential range –0.15 to 0.15 V(RHE), the anodic current transients display first a linear relationship between logarithmic current and logarithmic time with a slope of –0.5 and then an exponential decay with time, indicating the Cottrell behaviour. This means that the hydrogen transport through the electrode proceeds in the presence of single α-PdH_δ phase and at the same time hydrogen concentration c_H at the electrode surface is fixed at zero, corresponding to the discharging potential 0.9 V(RHE). Moreover, the values of δ obtained from the anodic current transients do not exceed the maximum solubility of α-PdH_δ phase, 0.03. Therefore, it is suggested that α-PdH_δ phase is still stable above –0.15 V(RHE).

In this work, we assume that the hydrogen transport through the electrode is purely controlled by hydrogen diffusion in the electrode during the hydrogen extraction under the self-discharge and potentiostatic conditions. Thus, Fick's second law was employed as the governing equation for the hydrogen transport.

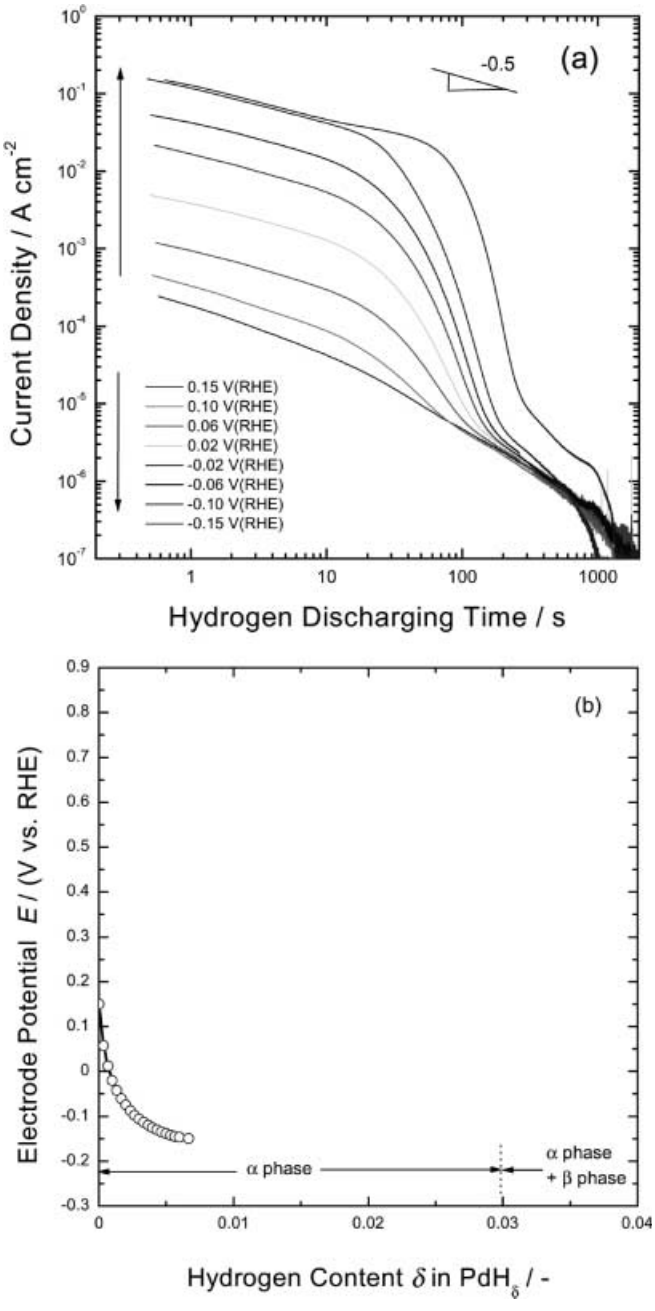

Fig. 1 **a** Anodic current transients on a logarithmic scale, log i vs log t obtained by jumping various hydrogen pre-charging potentials –0.15 to 0.15 V(RHE) to the hydrogen discharging potential 0.90 V(RHE). **b** Plot of the electrode potential E against the hydrogen content δ in the Pd foil electrode in 0.1 mol l^{-1} NaOH solution, obtained from the integration of the anodic transients **a** with respect to time

The kinetics of hydrogen transport during the OCP transient

Figure 2 shows OCP transient measured on Pd foil electrode in 0.1 mol l^{-1} NaOH solution from the moment just after interrupting the pre-charging potential of –0.02 V(RHE) for 2×10^3 s. The OCP transient displays first a steep rise and then a potential plateau, followed

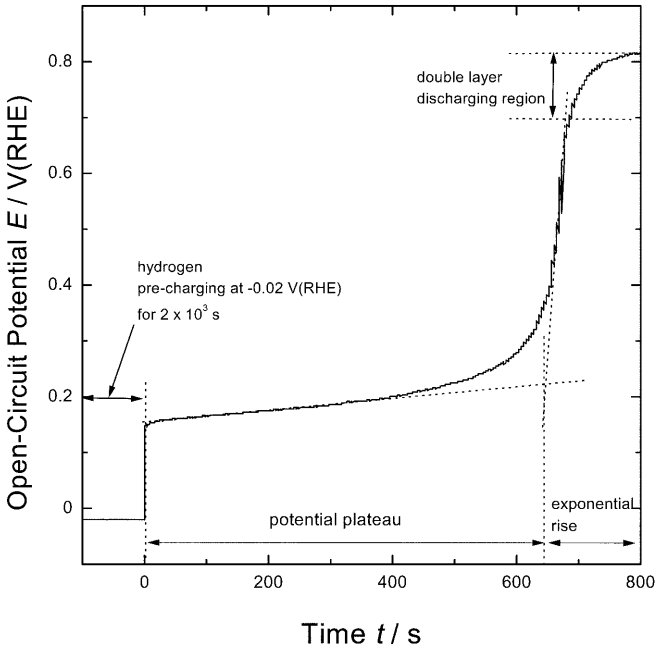

Fig. 2 OCP transient measured on Pd foil electrode in 0.1 mol l^{-1} NaOH solution from the moment immediately after interrupting the pre-charging potential of –0.02 V(RHE) for 2×10^3 s

by an exponential rise with time. According to the works reported elsewhere [10, 11, 12], the exponential rise of the OCP transient above 0.7 V(RHE) is attributed to the double layer discharging after hydrogen is completely extracted from the electrode.

The value of OCP measured below 0.7 V(RHE) is determined by Faradaic reaction including the hydrogen oxidation at the electrode surface and thus the OCP for hydrogen dissolution is analogous to the corrosion potential for the metal corrosion, which is well described by the mixed potential theory [13].

Figure 3 presents an Evans-Hoar diagram E vs log i for hydrogen dissolution reaction. Here the cathodic polarization curve is composed of three different regions. The first region involves the activation-controlled hydrogen underpotential deposition ($M + H_2O + e_\beta = MH_{ads} + OH^-$) below 0.15 V(RHE), the second region corresponds to the diffusion-controlled oxygen reduction ($1/2O_2 + H_2O + 2e_\beta = 2OH^-$) in the range 0.15 to 0.75 V(RHE), and the final region is the activation-controlled oxygen reduction above 0.75 V(RHE). As a conceivable anodic half-reaction, the hydrogen oxidation is suggested as $MH_{ads} + OH^- = M + H_2O + e_\alpha$.

Considering that the couple of hydrogen oxidation rate i_{corr}/corrosion potential E_{corr} is determined by exchange current density i_o in Fig. 3, it is necessary to obtain a time-dependent function of i_o in order to simulate the i_{corr}/E_{corr} transient. Taking into account that the value of i_o is proportional to the surface concentration of hydrogen c_H [14], it is readily expected that as hydrogen dissolution runs, the instantaneous surface coverage of hydrogen is actually diminished and hence the instantaneous i_o is lowered in value with time.

By using the change in i_o with time, the i_{corr}/E_{corr} transients can be easily calculated from the Evans-Hoar diagram in Fig. 3. The calculated i_{corr}/E_{corr} transients

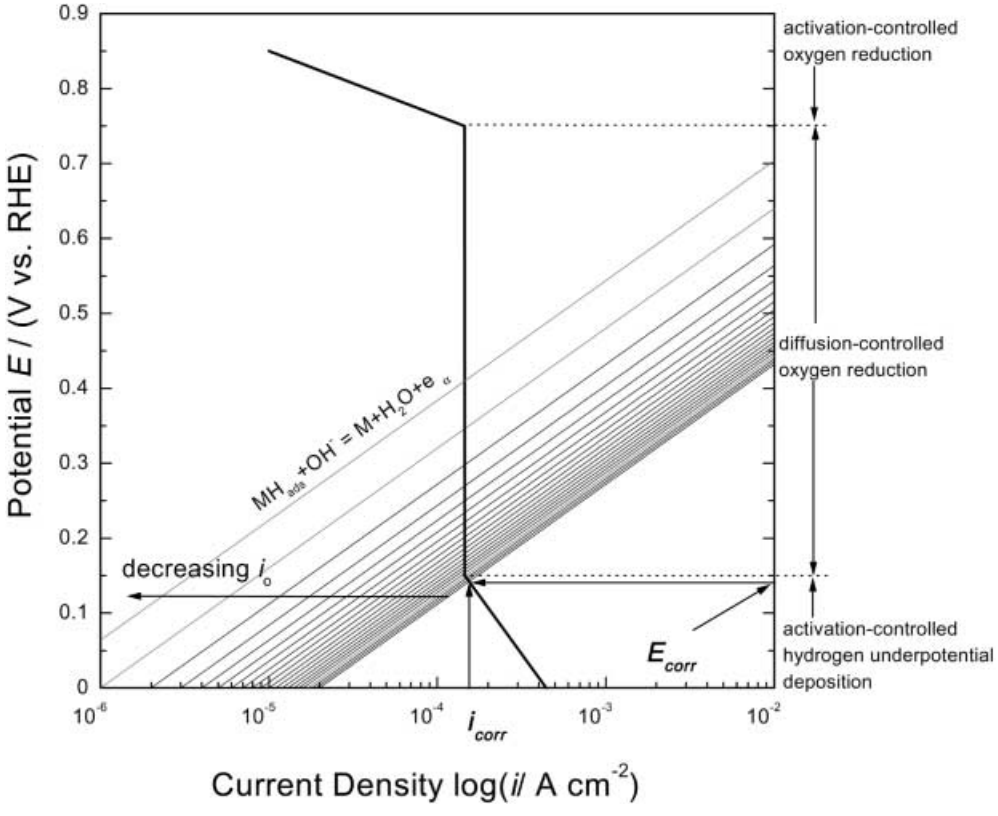

Fig. 3 Evans-Hoar diagram for the hydrogen dissolution reaction through an electrochemical mixed process. OCP is determined by a mixing of the potentials of two simultaneous reactions of anodic hydrogen oxidation and cathodic hydrogen underpotential deposition below 0.15 V(RHE) and oxygen reduction above 0.15 V(RHE), coupled by a common rate

are exhibited in Fig. 4. The computation process for the i_o and i_{corr}/E_{corr} transients have been detailed elsewhere [15]. The value of i_{corr} decreases linearly with time in the activation-controlled hydrogen underpotential deposition region, but it remains constant in the diffusion-controlled oxygen reduction region.

Comparing the E_{corr} simulated transient in Fig. 4 with the OCP transient measured in Fig. 2, it is seen that the simulated E_{corr} transient agrees well with the OCP transient measured below 0.7 V(RHE) in shape and value. This indicates that the simulated i_{corr} transient is coupled with the measured OCP transient. Consequently, we can determine the rate of the hydrogen self-discharge from the electrode during the OCP transient as the value of the simulated i_{corr}.

It is interesting to note that the horizontal potential plateau can even appear in the presence of single α-PdH_δ. This result is inconsistent with the suggestion that the potential plateau during the OCP transient originates from the 'quasi-equilibrium' between α-PdH_δ and β-PdH_δ [15, 16]. Considering that the electrode specimen pre-charged at –0.02 V(RHE) consists fully of α-PdH_δ, it can be asserted that the occurrence of horizontal potential plateau during the OCP transient is due not to the coexistence of α-PdH_δ and β-PdH_δ, but to the slow self-discharge rate.

During the OCP transient, the initial condition (I.C.) in the electrode and boundary condition (B.C.) at the electrode surface and the Au layer are expressed as follows:

$$\text{I.C.}: \quad c_H = c^o \quad \text{for} \quad 0 \le x \le L \quad \text{at} \quad t = 0 \tag{1}$$

$$\text{B.C.}: \quad -F\tilde{D}_H\left(\frac{\partial c_H}{\partial x}\right) = 0 \quad \text{for} \quad x = L \quad \text{at} \quad t > 0 \tag{2}$$

(impermeable constraint)

and

$$\text{B.C.}: \quad -F\tilde{D}_H\left(\frac{\partial c_H}{\partial x}\right) = i_{corr}(t) \quad \text{for} \quad x = 0 \quad \text{at} \quad t > 0 \tag{3}$$

(constraint by hydrogen self-discharge rate)

Here, F is the Faraday constant; $\tilde{D}_H$, the chemical diffusivity of hydrogen; c_H, the hydrogen concentration, and $i_{corr}(t)$ represents the transient of hydrogen self-discharge rate.

By combining Fick's second law with the initial condition (Eq. 1) and the boundary conditions (Eqs. 2 and 3), the hydrogen concentration profile transient was numerically calculated where $\tilde{D}_H$ was taken as 3×10^{-7} cm^2 s^{-1} [17, 18, 19] and $i_{corr}(t)$ was used as i_{corr} transient given in Fig. 4. The result is illustrated in Fig. 5. The concentration gradient at the electrode surface diminishes linearly with time in the activation-controlled hydrogen underpotential deposition region, but it retains constant value in the diffusion-limited oxygen reduction region.

The kinetics of hydrogen transport during the anodic current transient

Figure 6 depicts anodic current transients on a logarithmic scale, obtained from Pd foil electrode in 0.1 mol l^{-1} NaOH solution by jumping the pre-charging potential of –0.02 V(RHE) to various discharging potentials E_D ranging from 0.2 to 0.9 V(RHE). It should be noted that the amount of hydrogen pre-charged in the electrode Q was calculated by integrating the anodic current transient with respect to time and it shares almost the same value of about 8.2×10^{-2} C cm^{-2}, irrespective of the value of E_D.

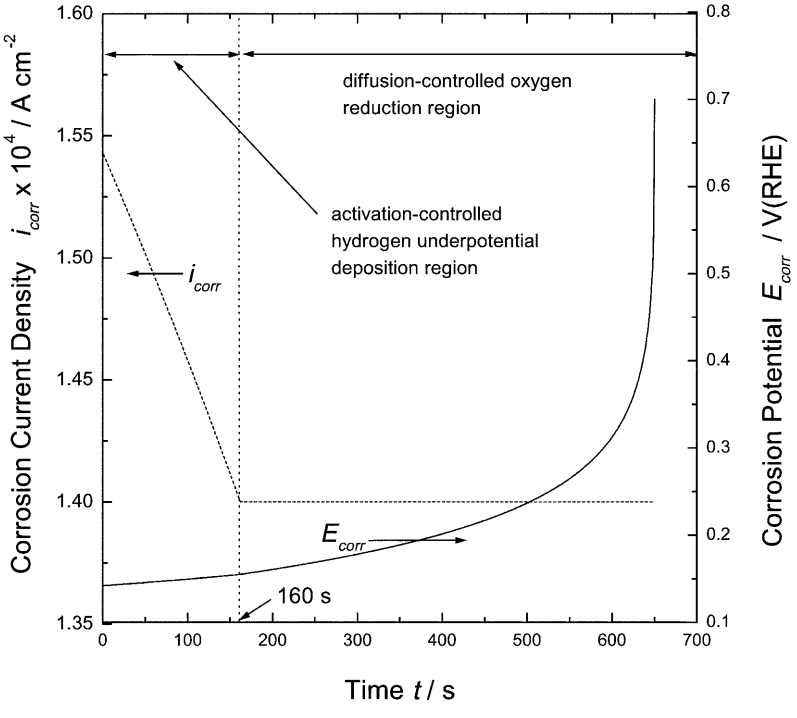

Fig. 4 Couple of i_{corr} transient and E_{corr} transient, calculated theoretically from the Evans-Hoar diagram in Fig. 3 by using i_o transient

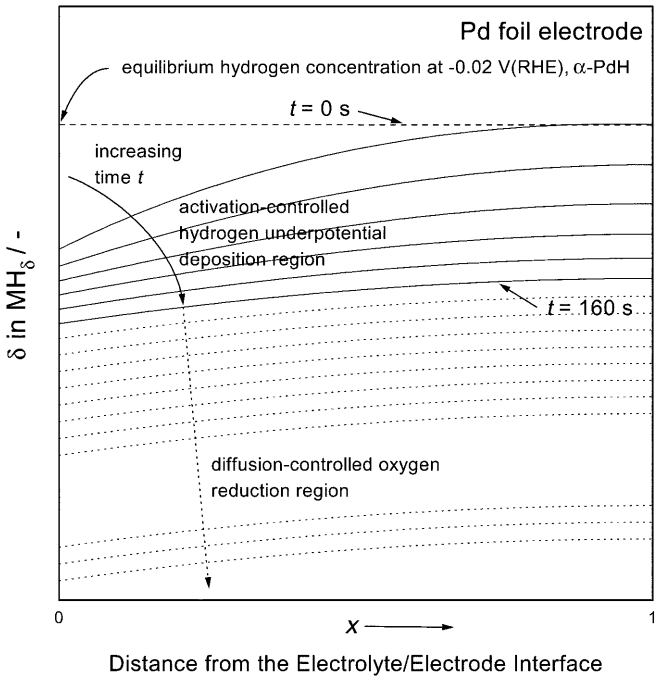

Fig. 5 Hydrogen concentration profile transient during the OCP transient of Fig. 2, determined from the numerical solution to Fick's second law under the initial condition (Eq. 1) and the boundary conditions (Eqs. 2 and 3)

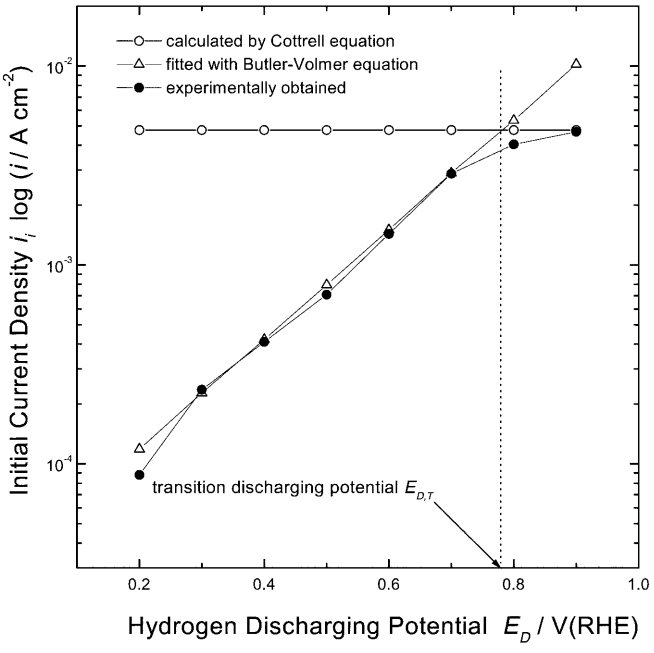

Fig. 7 Plot of initial current density i_i against the hydrogen discharging potential E_D, obtained from Pd foil electrode pre-charged with hydrogen at –0.02 for 2×10^3 s: *open circle*, i_i at 0.5 s calculated by the Cottrell equation; *triangle*, i_i fitted with the Butler-Volmer equation; *filled circle*, measured i_i at 0.5 s obtained from Fig. 6

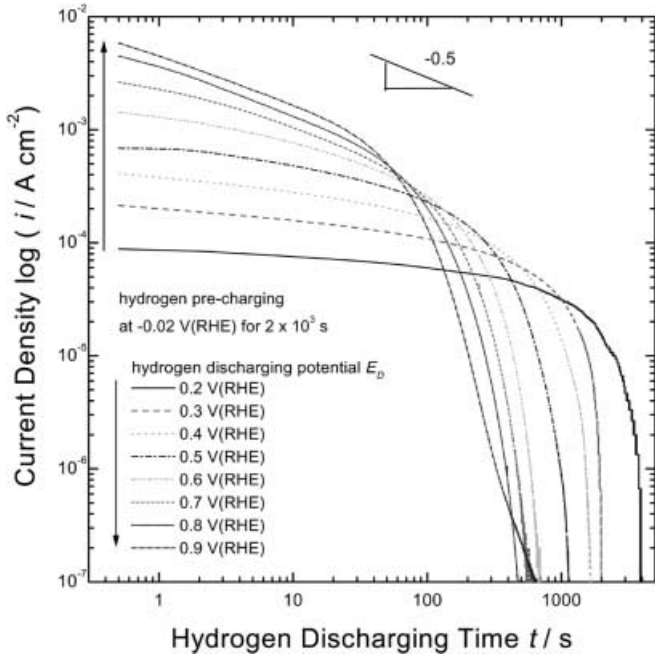

Fig. 6 Anodic current transients on a logarithmic scale, measured on Pd foil electrode in 0.1 mol l^{-1} NaOH solution by jumping the pre-charging potential of –0.02 V(RHE) to various discharging potentials ranging from 0.2 to 0.9 V(RHE)

In the high discharging potential E_D range of 0.8 to 0.9 V(RHE), the anodic current transient shows clearly a linear relationship between logarithmic current and logarithmic time with a slope of –0.5, followed by an exponential decay with time, indicating the Cottrell behavior. This implies that c_H at the electrode surface is fixed to a constant value corresponding to E_D, as mentioned in Fig. 1a. Figure 1b showed that the surface concentration c_H becomes to zero when the electrode surface is subjected to the potentials E_D 0.8 and 0.9 V(RHE). However, in the low discharging potential E_D range 0.2 to 0.7 V(RHE), the logarithmic current transient shows a current plateau and then an exponential decay with time. As E_D rises, the slope of the logarithmic current transient increases progressively from zero to –0.5.

The initial current density i_i obtained at 0.5 s from Fig. 6 is envisaged on a semi-logarithmic scale in Fig. 7 against E_D. In Fig. 7 the logarithmic i_i increases linearly with rising E_D up to 0.8 V(RHE) and then remains nearly constant. By employing the value of Q as 8.2×10^{-2} C cm^{-2} measured from Fig. 6, we calculated the value of i_i at 0.5 s from the Cottrell equation for the short time region [4, 5]. The calculation of i_i at 0.5 s yielded 4.8×10^{-3} A cm^{-2} for the potential jump of –0.02 V(RHE) to E_D, which remains constant, regardless of E_D. The calculated values (open circles) are designated in Fig. 7 along with the measured values (filled circles).

The measured and calculated values almost duplicate each other above 0.8 V(RHE). However, the measured and calculated values do not coincide below 0.8 V(RHE). Below 0.8 V(RHE), the measured values of i_i can be well fitted to i_i theoretically calculated from the Butler-Volmer equation [13, 14] by assuming the parameters exchange current density $i_o = 1.0\times10^{-5}$ A

cm^{-2} and transfer coefficient for the hydrogen reduction $\alpha = 0.64$. The values of i_o and α are in agreement with those values measured by Enyo and Biswas [20].

Figure 7 showed that the one constraint to another transition potential $E_{D,T}$ is determined as the discharging potential E_D at which the i_i vs E_D curve calculated by the Cottrell equation intersects that curve fitted with the Butler-Volmer equation.

During the anodic current transient, I.C. in the electrode and B.C. at the electrode surface and the impermeable interface are summarized as follows:

$$\text{I.C.}: \quad c_H = c^o \quad \text{for} \quad 0 \le x \le L \quad \text{at} \quad t = 0$$

$$\text{B.C.}: \quad -F\tilde{D}_H\left(\frac{\partial c_H}{\partial x}\right) = 0 \quad \text{for} \quad x = L \quad \text{at} \quad t > 0$$

(impermeable constraint)
and

$$\text{B.C.}: -F\tilde{D}_H\left(\frac{\partial c_H}{\partial x}\right) = i_o\left[e^{-\frac{\alpha F}{RT}(E_D - E)} - e^{\frac{(1-\alpha)F}{RT}(E_D - E)}\right] \quad \text{for } x = 0 \text{ at } t > 0 \tag{4}$$

(constraint by Butler-Volmer behaviour) below $E_{D,T}$, (Eq. 2) (impermeable constraint) and

$$\text{B.C.}: \quad c_H = 0 \quad \text{for} \quad x = 0 \quad \text{at} \quad t > 0 \tag{5}$$

(constraint of the constant concentration) above $E_{D,T}$.

Here, (E_D–E) is the actual potential jump. The notations R and T are usually used symbols. Figure 1b showed that as hydrogen is extracted from the electrode, the actual potential jump (E_D–E) in (Eq. 4) decreases more rapidly. Thus, the concentration gradient $\left(\frac{\partial c_H}{\partial x}\right)_{x=0}$ at the electrode surface decreases more rapidly to a negligible small value according to (Eq. 4).

By using the initial condition (Eq. 1) and the boundary conditions (Eqs. 2 and 4) below $E_{D,T}$, the anodic current transient and hydrogen concentration profile transient were numerically calculated, which are demonstrated in Fig. 8a,b, respectively. Two remarks should be made about the simulated anodic current transients. In the first place, the higher E_D is, the higher value has the logarithmic initial current density progressively. In the second place, the higher E_D is, the more markedly increases the value of the slope of logarithmic current density.

Comparing the simulated anodic current transients with those measured below $E_{D,T}$ in Fig. 6, in view of the two remarks made above, it is found that the simulated anodic current transients coincide well with those measured. As a consequence, the boundary condition by Butler-Volmer behavior at the electrode surface is valid for the anodic current transient below $E_{D,T}$. Below $E_{D,T}$, c_H at the electrode surface is not fixed to zero, but changes with time.

By employing the initial condition (Eq. 1) and the boundary conditions (Eqs. 2 and 5) above $E_{D,T}$, the anodic current transient and hydrogen concentration profile transient were simulated, which are given in Fig. 9a,b, respectively. A good agreement of the anodic current transient calculated in Fig. 9a with that measured above $E_{D,T}$ in Fig. 6 indicates that the constant concentration condition at the electrode surface is effective for the anodic current transient above $E_{D,T}$. In this case, c_H at the electrode surface is fixed

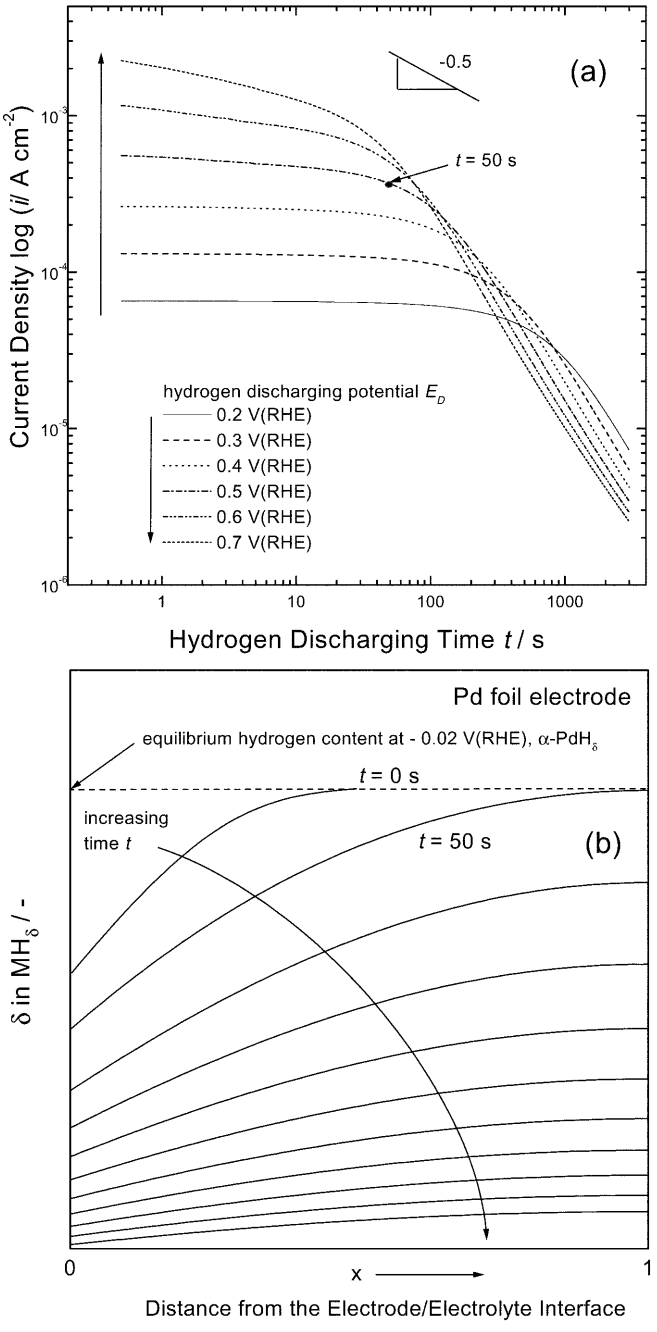

Fig. 8 **a** Anodic current transients at the potential jumps of –0.02 V(RHE) to various discharging potentials ranging from 0.2 to 0.7 V(RHE). **b** Hydrogen concentration profile transient at the potential jump of –0.02 V(RHE) to 0.5 V(RHE), determined from the numerical solution to Fick's second law under the initial condition (Eq. 1) and boundary conditions (Eqs. 2 and 4)

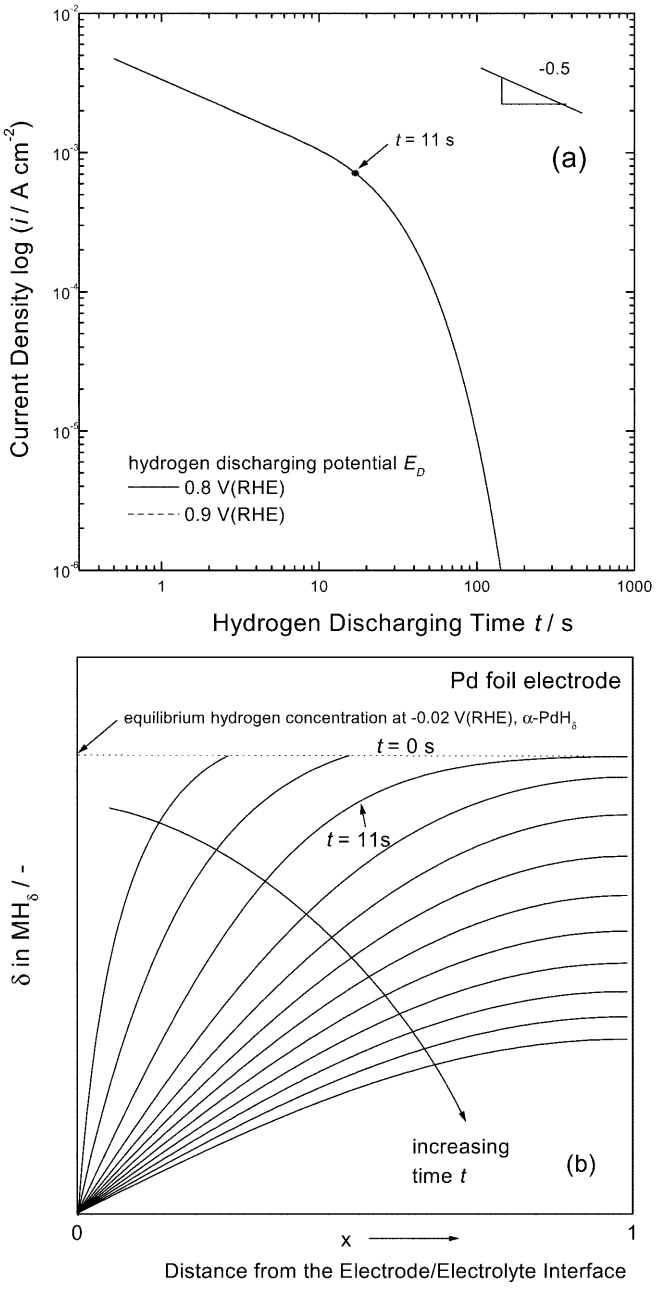

Fig. 9 **a** Anodic current transient at the potential jump of –0.02 V(RHE) to the discharging potentials of 0.8 and 0.9 V(RHE). **b** Hydrogen concentration profile transient at the potential jump of –0.02 V(RHE) to 0.9 V(RHE), determined from the numerical solution to Fick's second law under the initial condition (Eq. 1) and boundary conditions (Eqs. 2 and 5)

to zero, corresponding to E_D during the hydrogen extraction.

In conclusion, the hydrogen oxidation rate transient simulated on the basis of the mixed potential theory represents the self-discharge rate during the OCP transient. When the electrode surface is subjected even to a constant discharging potential E_D, c_H corresponding to E_D is fixed to zero at the electrode surface above the transition discharging potential $E_{D,T}$, but the change of concentration gradient at the electrode surface with time is specified by Butler-Volmer behaviour below $E_{D,T}$. By employing the hydrogen oxidation rate during the OCP transient and the two constraints during the anodic current transient as the boundary condition at the electrode surface, we present the variation of hydrogen concentration profile across the electrode with time during the hydrogen extraction under the self-discharge and potentiostatic conditions, respectively.

Acknowledgements The present work has been carried out under the auspices of the joint program of Korea Science and Engineering Foundation (KOSEF) and Japan Society for the Promotion of Science (JSPS) 1999/2001. The authors are indebted to KOSEF for the financial support of this work. Furthermore, this work was partly supported by the Brain Korea 21 project.

References

1. Han J-N, Pyun S-I, Yang T-H (1997) J Electrochem Soc 144:4266
2. Iwakura C, Oura T, Inoue H, Matsuok M, Yamamoto Y (1995) J Electroanal Chem 398:37
3. Wang X-L, Suda S, Wakao S (1994) Z Phys Chem 183:297
4. Wen CJ, Boukamp BA, Huggins RA, Weppner W (1979) J Electrochem Soc 126:2258
5. Yoon Y-G, Pyun S-I (1997) Electrochim Acta 42:2465
6. Ura H, Nishina T, Uchida I (1995) J Electroanal Chem 396:169
7. Zhou Z, Huang J, Hu W, Yao F, Zhang Y (1995) J Alloys Compd 231:297
8. Pyun S-I, Han J-N, Yang T-H (1997) J Power Sources 65:9
9. Mueller M, Blackledge JP, Libowitz GG (1968) Metal hydrides. Academic Press, New York, p 547
10. Macdonald DD (1977) Transient techniques in electrochemistry. Plenum Press, New York, p 119
11. Gu P, Bai L, Brousseau R, Conway BE (1992) Electrochim Acta 37:2145
12. Gileadi E (1993) Electrode kinetics. VCH, New York, p 349
13. Wagner C, Traud W (1938) Z Elektrochem Ang Phys Chem 44:391
14. Bard AJ, Faulkner LR (1980) Electrochemical methods. Wiley, New York, p 103
15. Han J-N, Pyun S-I (2000) Electrochim Acta 45:2781
16. Yang T-H, Pyun S-I, Yoon Y-G (1997) Electrochim Acta 42:1701
17. Devanathan MAV, Stachurski Z (1962) Proc R Soc 270:90
18. Lim C, Pyun S-I (1993) Electrochim Acta 38:2645
19. Lee WJ, Pyun S-I, Yang T-H, Kim J-D, Baek Y-H, Kim H-G (1997) J Solid State Electrochem 1:120
20. Enyo M, Biswas P (1992) J Electroanal Chem 335:309